Dalton Transactions

ROYAL SOCIETY OF CHEMISTRY

PAPER

View Article Online
View Journal | View Issue

Cite this: *Dalton Trans.*, 2026, **55**, 3266

Construction of three-dimensional hierarchical flower-like M(OH)(OCH_3) (M = Co and Cu) microspheres for high efficiency electrocatalytic oxygen evolution

Pan Yang,[a] Congmin Fan, *[a] Tiancheng Feng,[a] Haoyu Peng,[a] Xiaolian Xu[a] and Guiqi Gao*[b]

Received 10th November 2025,
Accepted 17th January 2026

DOI: 10.1039/d5dt02687c

rsc.li/dalton

The slow kinetics of the oxygen evolution reaction hinders the efficiency of water decomposition, so it is crucial to develop noble metal-free electrocatalysts for the efficient decomposition of water *via* the oxygen evolution reaction (OER) in alkaline electrolytes. In this study, flower-like structured hydroxides grown *in situ*, consisting of ultrathin nanosheets stacked on Fe Foam (FF), were prepared by a one-step hydrothermal method for an efficient electrocatalytic oxygen evolution reaction. M(OH)(OCH_3) (M = Co and Cu) requires only a low overpotential of 270 mV and 379 mV for the OER, to provide 20 mA cm^{-2} and 100 mA cm^{-2} current densities, respectively. With the synergistic effect of Co^{2+} and Cu^{2+}, the adsorption capacity of the intermediate OH* and the conductivity are improved, and the structural surface reconstruction is promoted by methoxide. In this work, the structure of FF-based electrocatalysts was modulated by the introduction of Co^{2+} and Cu^{2+} and the formation of methoxy anions, which improved the catalytic activity of the catalysts.

1. Introduction

The world is facing two key issues that impact sustainable development: the crisis of shortage of traditional fossil energy sources and the environmental pollution caused by the burning of fossil fuels.[1–4] To address these issues, both academia and industry are exploring renewable energy sources for replacing traditional fossil fuels, and among the most promising energy sources is hydrogen energy, owing to its high energy density and excellent environmental credentials.[5,6] Hydrolysis technology, supported by renewable energy sources such as solar or wind power, offers a powerful way to support the sustainable production of hydrogen.[7–9] Electrochemical water decomposition in alkaline media, in which the hydrogen evolution reaction (HER) occurs at the cathode and the oxygen evolution reaction (OER) at the anode, is a promising method for large-scale, cost-effective hydrogen production.[10] However, the slow kinetics of the OER remains an important difficulty in the overall water decomposition process because oxygen evolution requires four negative charge transfer processes compared to the two negative charge transfer processes required for hydrogen evolution.[11] In order to decrease the overpotential, researchers have investigated a variety of OER noble metal-based electrocatalysts. However, their large-scale industrial application is constrained by their additional costs and limited availability.[12]

During the OER process, the catalyst at the anodic polarization potential is easily oxidized; the cobalt (oxygen) hydroxide formed on the catalyst surface is extensively used as an active substance. For example, it has been discovered that atomically thin cobalt hydroxide oxide (γ-CoOOH) containing abundant defects exhibits outstanding water oxidation performance.[13] The existence of numerous defects altered the state of the Co 3d valence electron configuration effectively and thus optimized the intrinsic activity of active sites. According to the available studies, the Jahn–Teller effect of Cu^{2+} effectively increases the conductivity and accelerates the charge transfer of the samples, which plays an important role in improving the electrocatalytic activity.[14,15]

However, their active sites are limited due to the layered structure of the stack; therefore, the experimentally measured onset potentials of cobalt(oxy)hydroxides are much larger than the thermodynamic equilibrium potentials.[16] According to existing research, introducing strongly electronegative anionic groups induces surface restructuring, thereby enhancing active sites and improving electrocatalytic activity. For example, a novel layered cobalt compound Co(OH)(OCH_3)[17] has been

[a]*College of Materials and Chemistry & Chemical Engineering, Chengdu University of Technology, Chengdu 610059, China. E-mail: fcongmin@mail.ustc.edu.cn*
[b]*Institute of Physical Science and Information Technology, Anhui University, Hefei, 230601, China. E-mail: gaogq@ahu.edu.cn*

reported, where the anionic ligand (methoxy) replaces the half hydroxyl of β-$Co(OH)_2$, exhibiting superior OER electrocatalytic performance. Due to the higher electronegativity of methoxy, its high electron-withdrawing ability readily induces the formation of higher-valent metal ions.[13,18] Surface restructuring of the OER catalyst can be modulated due to thermodynamically driven anion substitution reactions involving hydroxyl groups.[19–22] Furthermore, the larger molecular size of the methoxy group facilitates expansion of the interlayer spacing, exposing more active sites.[23]

In this paper, the flower-like structured bimetallic compounds $M(OH)(OCH_3)$ (M = Co and Cu) (marked as CoCuMe) were synthesized by a one-step hydrothermal method consisting of ultrathin nanosheets stacked on top of each other. It was shown that the incorporation of cobalt and copper ions and the introduction of methoxy anions on an Fe foam substrate induced the modulation of the electronic structure of the surface as well as the improvement of the microstructure. Because of the synergistic effect of these ions, the overpotential of CoCuMe is only 270 mV, and the current density can reach 20 mA cm^{-2}, which is 50 mV and 61 mV lower than those of the CoMe (318 mV) and CuMe (329 mV) samples, respectively. The overpotential is further reduced by 105 mV compared to the blank sample of Fe foam (373 mV).

2. Experimental section

2.1. Synthesis of catalysts

Fe Foam (FF) was selected from Kunshan Xingzhenghong Electronic Materials. Hexahydrate cobalt nitrate ($Co(NO_3)_2{\cdot}6H_2O$) and anhydrous copper chloride ($CuCl_2$) were purchased from Shanghai Aladdin Biochemical Science and Technology. The reagents used were analytically pure, and the water used in the experiments was deionized.

2.2. Material characterization

The Fe foam was pretreated by cutting it into a 1 cm × 2 cm piece, immersing in an appropriate amount of anhydrous ethanol, and ultrasonicated in an ultrasonic machine for 15 minutes. Then, it was transferred into an appropriate amount of deionized water and ultrasonicated for an additional 15 minutes.

$M(OH)(OCH_3)$ (M = Co and Cu) (marked as CoCuMe) was synthesized according to a one-step hydrothermal method. 0.2 mmol cobalt nitrate and 0.1 mmol copper chloride were dissolved in 25 ml of methanol and stirred for 10 min until the solute was completely dissolved in the solution. Fe Foam was transferred to a 100 ml hydrothermal autoclave and the dissolved colored solution was placed in the hydrothermal autoclave. The solution was placed in a drying oven and reacted at 180 °C for 12 hours. The sample was taken out and the material on the surface of the sample was rinsed with deionized water. Then, the sample was placed in a drying oven and dried at 60 °C for 5 minutes.

The comparison samples, $M(OH)(OCH_3)$ (M = Co) (CoMe) and $M(OH)(OCH_3)$ (M = Cu) (CuMe), were prepared in the same way; the solute of CoMe was 0.2 mmol cobalt nitrate, and the solute of CuMe was 0.1 mmol copper chloride.

2.3. Electrochemical measurement

In this study, a three-electrode test method was used, and all electrochemical tests were carried out using a CHI 760E electrochemical workstation (Chenhua, Shanghai, China) in an alkaline solution of 1 M KOH at room temperature. The working electrode consists of the catalyst prepared in this work, with a platinum electrode serving as the counter electrode and a mercury oxide electrode (Hg/HgO) acting as the reference electrode. The potential of the reversible hydrogen electrode can be converted from the measured potential using the Nernst equation ($E_{RHE} = E_{Hg/HgO} + 0.098\ V + 0.059\ pH$). All LSV curves were tested at a scan rate of 5 mV s^{-1} with 100% iR compensation. The geometric surface area of the samples was used for current density normalization. Electrochemical impedance spectroscopy (EIS) was measured in the frequency range of 10^{-2} to 10^5 Hz, which was used to explore the internal resistance of different samples. Cyclic voltammetry (CV) was used to evaluate the double-layer capacitance (CDL), and stability tests were also performed by chronoamperometry.

2.4. Characterization

Using X-ray diffraction (XRD, Ultima IV diffractometer, Rigaku), the crystal structure of the prepared catalysts was investigated in the 2θ scanning range of 5–80°. The surface morphology of the catalyst was analyzed by scanning electron microscopy (SEM, Hitachi SU8010). Energy dispersive X-ray spectroscopy (EDS) was performed to analyze the elemental distribution of the materials. Transmission electron microscopy (TEM, FEI Tecnai G2 F20 200 kV) was employed to further investigate the microstructure of the catalysts. The valence state information of the material surface was investigated using an X-ray photoelectron spectrometer (XPS, Thermo K-Alpha) equipped with an Al-Kα (1486.6 eV) radiation source, and the result of the C 1s spectral line at 284.8 eV was corrected.

3. Results and discussion

3.1. Synthesis and characterization of CoCuMe

The synthesis of CoCuMe is shown in Fig. S1 (Fig. S1, SI). CoCuMe was synthesized by a one-step hydrothermal method, in which cobalt nitrate served as the cobalt source, copper chloride served as the copper source, and a methanol solution was used as the solvent. For comparison, CoMe and CuMe were also prepared. Firstly, X-ray diffraction (XRD) was used to analyze the crystalline phases of the three materials. The patterns are shown in Fig. 1. For the spectrum of CoCuMe, the peaks at 11.31°, 23.84°, 32.21° and 39.44° can be found clearly corresponding to the (003), (006), (101), (015) and (018) planes, respectively. The OH^- and OCH_3^- peaks obtained during the preparation process correspond to all characteristic peaks of CoCuMe observed in Dong's XRD study.[24] From the spectrum

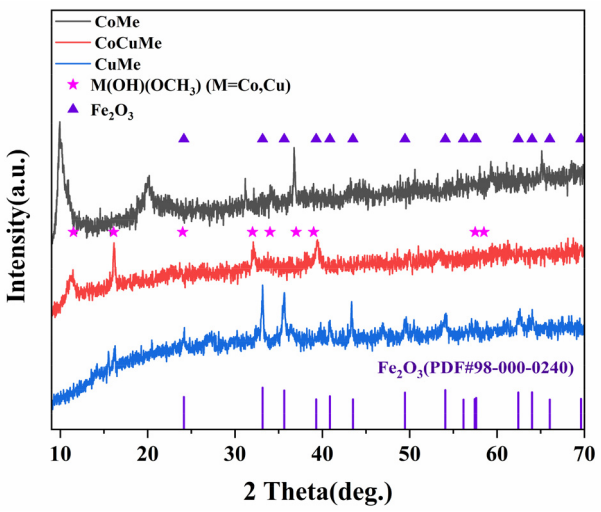

Fig. 1 Comparison of the XRD patterns of M(OH)(OCH_3) (M = Co, Cu).

of CuMe, the peak of Fe_2O_3 can be clearly seen, and a small amount of the Fe_2O_3 crystalline phase was present in the spectra due to the fact that the Fe foam substrate is very active in air and the added Cu^{2+} has the ability to promote the oxidation of low-valent cations to high-valent cations and can oxidize Fe^{2+} to Fe^{3+}. The weak peaks indicate the poor crystallinity of the metal hydroxymethylated materials synthesized by a solvothermal method.[10]

The microscopic morphology of CoCuMe was observed by scanning electron microscopy (SEM) (Fig. 2a and b). The SEM of CoMe and CuMe was used for comparison (Fig. S2). CoMe is formed by the stacking of large particles with diameters of 1 μm and 5 μm, while CuMe is composed of cubes with edge lengths of approximately 1 μm. CoCuMe showed a flower-like structure consisting of ultrathin nanosheets stacked on top of each other.[25]The thickness of the CoCuMe nanosheets was about 50 nm, and compared to the SEM of CoMe and CuMe (Fig. S2), the microstructure of CoCuMe could expose more active sites and was easier for cation attachment for a better catalytic effect. With the introduction of Fe^{3+} ions, well-defined ultrathin nanosheets can be formed on the substrate, and the released Fe also regulates the mixed valence states of metal ions in hydroxides, which significantly enhances the material's electrical conductivity.[15,26,27] Transmission electron microscopy (TEM) images further confirmed the ultrathin nature of CoCuMe nanosheets (Fig. 2d). In the high-resolution TEM (HRTEM) images, the lattice stripes with crystallographic spacings of 0.197 nm and 0.234 nm corresponded better to the (018) and (015) planes, respectively (Fig. 2e). The energy dispersive spectroscopy (EDS) elemental mapping images demonstrate the uniform distribution of the elements Fe, Co, Cu, and O in the measurement region (Fig. 2c). Since Co and Cu elements are homogeneously dispersed on the Fe foam substrate, it can be confirmed that we successfully synthesized the bimetallic hydroxymethyl compound sample. According to the existing literature, the elemental molar ratios of different elements also affect the electrocatalytic properties of the samples.[25] Fe, Co and Cu are transition metals, and these ions have stronger polarization (or oxygen affinity) and can form more stable metal–oxygen covalent bonds in the metal hydroxymethyl compounds.

The chemical states and binding energy data of different elements in CoCuMe, CoMe and CuMe were studied by X-ray photoelectron spectroscopy (XPS). The binding energy data are listed in Table S1. In the Fe 2p spectrum of CoCuMe, the peak at 709.60 eV corresponds to Fe^{2+} and the peak at 711.30 eV corresponds to Fe^{3+} (Fig. S4).[28] The binding energies of Fe^{2+} relative to CoMe and CuMe were positively shifted by 0.12 eV and 0.05 eV, the binding energies of Fe^{3+} relative to CoMe and CuMe were positively shifted by 0.20 eV and 0.12 eV. The molar ratios of Fe^{3+}/Fe^{2+} increased from 1.35 and 1.31 to 1.52. The data of the molar ratios are listed in Table S1. As shown in Fig. 3a, the peaks in the Co 2p spectra of CoCuMe, located at 780.38 (Co $2p_{3/2}$) and 795.43 (Co $2p_{1/2}$), the two sets of peaks at 783.78 (Co $2p_{3/2}$) and 796.91 (Co $2p_{1/2}$) correspond to Co^{3+} and Co^{2+}, respectively. The binding energies were increased by 0.12 eV, 0.15 eV, 1.63 eV, and 0.17 eV compared to those of CoMe at Co $2p_{3/2}$ and Co $2p_{1/2}$, respectively.[29] The molar ratio of Co^{3+}/Co^{2+} increased from 1.45 in CoMe to 1.74 in CoCuMe (Table S1). In the Cu 2p spectra of CoCuMe, the peak at 932.76 eV (Cu $2p_{3/2}$) corresponds to Cu^{2+} (Fig. 3b).[20] The binding energy of Cu^{+} and Cu^{2+} at Cu $2p_{1/2}$ and Cu $2p_{3/2}$ is positively shifted by 0.60 eV, 0.92 eV, 0.15 eV and 1.00 eV compared with that of CuMe (Table S1). The molar ratio of Cu^{3+}/Cu^{2+} increased from 1.62 in CuMe to 1.91 in CoCuMe (Table S1). The synergistic effect of Co^{2+} and Cu^{2+} causes a shift in the binding energy and contributes to the improvement of electrocatalytic OER activity. The O 1s of the CoCuMe spectrum is well divided into 532.18 eV of absorbed water (H_2O), 531.44 eV of oxygen defects (O_V), 530.70 eV of hydroxyl groups (OH), and 529.31 eV of lattice oxygen (M–O) (Fig. S4).[21]The O_V/M–O molar ratio of CoCuMe is 2.68, which is significantly higher than that of CoMe with an O_V/M–O molar ratio of 0.66 for CoMe and an O_V/M–O molar ratio of 0.28 for CuMe (Table S1), reflecting that the synergistic effect of Co and Cu elements also increases the molar ratio of oxygen vacancies in CoCuMe.[22,30,31] The oxidation of Co^{2+} to the higher valence Co^{3+} was promoted due to the introduction of Cu^{2+}, and in order to balance the reaction, anions (OCH_3^- and OH^-) were formed,[23] facilitating charge transfer and thereby enhancing electrocatalytic performance. From this result, it can be concluded that the simultaneous presence of cobalt-copper ions contributes to the conversion of Fe^{2+} to Fe^{3+} only, which facilitates the valence elevation of cobalt ions, enhances the molar ratio of Co^{3+}/Co^{2+} to a certain extent, and thus improves the electrochemical catalytic performance.

3.2. Investigation of the electrocatalytic OER performance of CoCuMe

A series of electrochemical tests were conducted to investigate the OER electrocatalytic activity of the prepared samples. Before being used as electrocatalysts, CoCuMe loaded on Fe

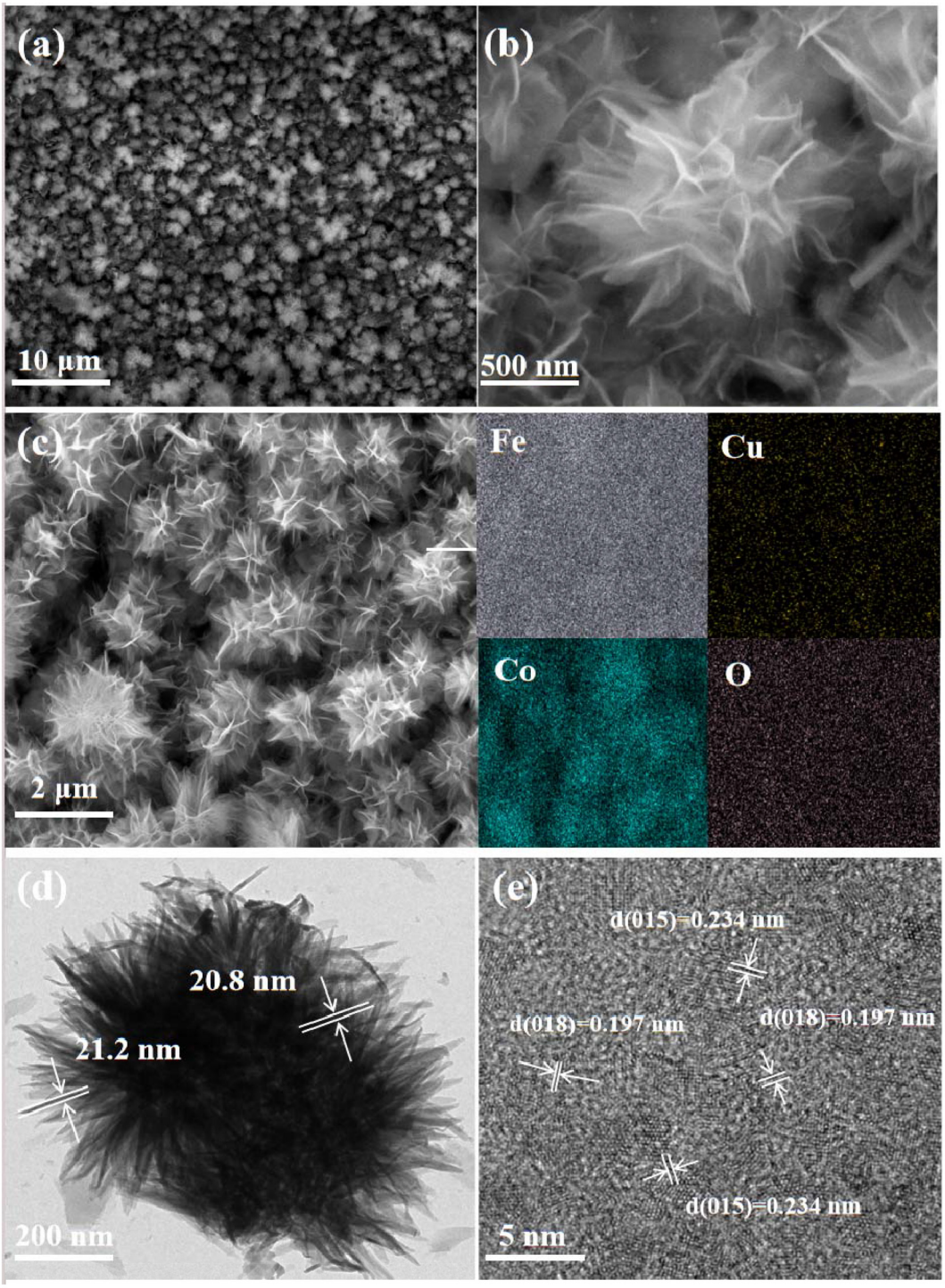

Fig. 2 (a and b) SEM images of CoCuMe, (c) SEM images and EDS elemental maps of CoCuMe, (d) TEM image of CoCuMe, and (e) HRTEM image of CoCuMe.

Foam (FF) was activated by continuous cyclic voltammetry (CV) scanning in a standard three-electrode system in 1 M KOH solution, and blank FF was used for comparison. A linear scanning voltammetry (LSV) test was carried out, in which a scan rate of 5 mV s^{-1} was used. As can be obtained from Fig. 4(a and b), the OER catalytic performance of CoCuMe was significantly better than those of CoMe, CuMe, and FF. The overpotentials of CoCuMe at current densities of 20 mA cm^{-2} and 100 mA cm^{-2} were only 270 mV and 379 mV (Fig. 4b), which were much lower than those of CoMe, CuMe and FF at the same current densities, which were 318 mV and 400 mV; 327 mV and 405 mV; and 370 mV and 434 mV (Fig. 4b).

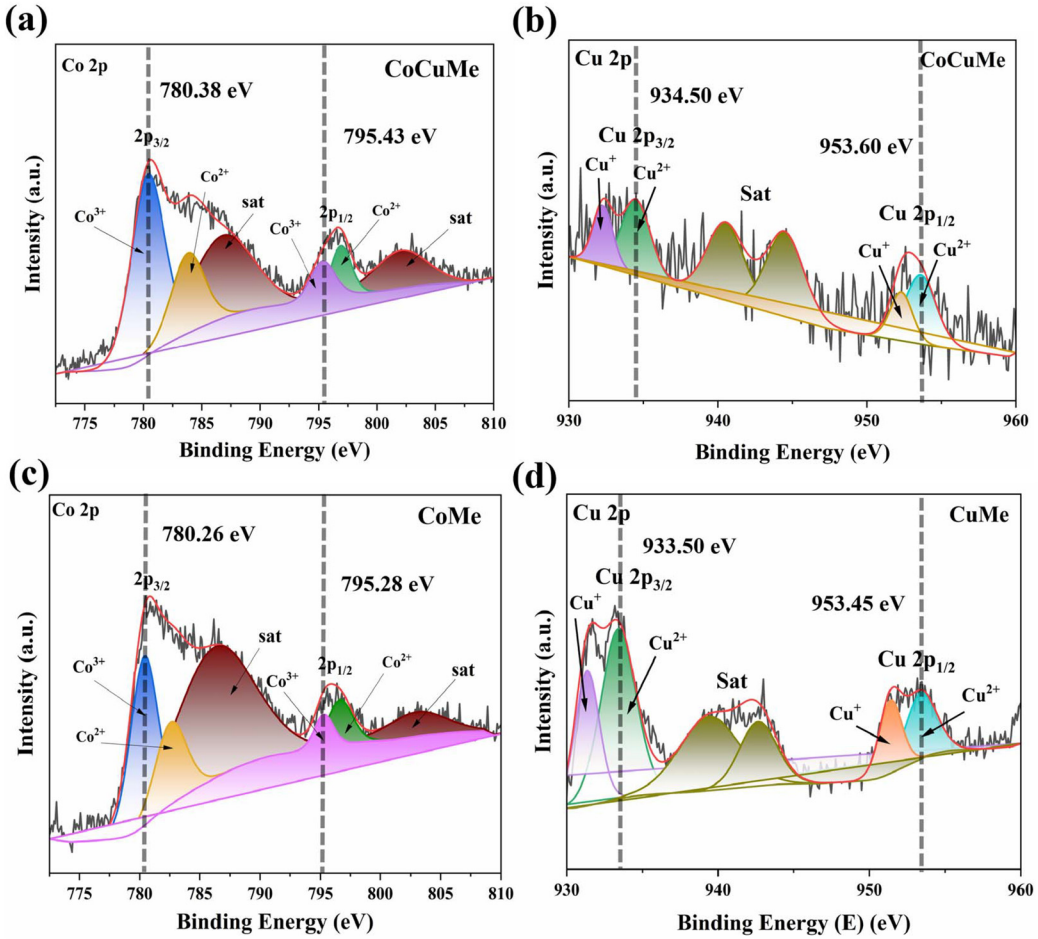

Fig. 3 High-resolution XPS spectra of Co 2p and Cu 2p of CoCuMe (a and b), Co 2p of CoMe (c), and Cu 2p of CuMe (d).

Therefore, it can be shown that the synergistic effect of Co and Cu brings about better electrocatalytic performance. The introduction of an appropriate amount of Cu^{2+} modulates the electronic structure of Co, and their synergistic effects are also crucial in influencing the performance of the electrocatalysts.[32]The Tafel slope can reflect the OER kinetics, and the Tafel slope was obtained by fitting the measured LSV curves, as shown in Fig. 4c. It can be seen that the Tafel slope of CoCuMe (34.53 mV dec^{-1}) is obviously smaller than that of CoMe (68.65 mV dec^{-1}) and CuMe (56.88 mV dec^{-1}). When the Tafel slope is smaller, the OER dynamics is more excellent, and thus the electrons can be transported more rapidly on the CoCuMe surface. This result also indicates that the catalytic performance of the OER is more favorable because low-valent cations are more readily oxidized to high-valent cations in CoCuMe, owing to the synergistic effect of Co^{2+} and Cu^{2+} in the electrocatalytic OER process. In order to further explore the influence of electrocatalytic kinetics on the catalytic performance of the OER, the electrochemical impedance spectra (EIS) of the samples were recorded and analyzed. In the energetic Nyquist plot shown in Fig. 4d, the charge transfer resistance (R_{ct}) is affected by the semicircular diameter in the high frequency region, and its value is one of the kinetic indicators of charge transfer between the electrode and the electrolyte. The semicircular diameters of the high-frequency region of the three samples measured, CoCuMe, CoMe, and CuMe, are 2.29 Ω, 4.69 Ω, and 16.77 Ω, which are obtained from the fitting results of the Nyquist plot in Table S2. It can be seen that the R_{ct} of CoCuMe is smaller than that of the other two samples, which leads to a higher electron transfer efficiency to enhance the electrocatalytic performance of the OER. According to the existing studies, the catalytic performance of metal hydroxymethoxides will be significantly improved by a higher proportion of valence metals, especially when the low valence ions can be converted to high valence ions during the OER process.[33] The results obtained in the above work well reflect this phenomenon. A comparison of the OER performance of CoCuMe catalysts reported in recent years is shown in Table S3. By comparing the overpotential data in Table S3, our prepared samples demonstrate lower overpotentials and superior electrocatalytic performance relative to recent non-precious metal research results.

The investigation of stability is also an important indicator, reflecting the electrochemical performance of the sample.

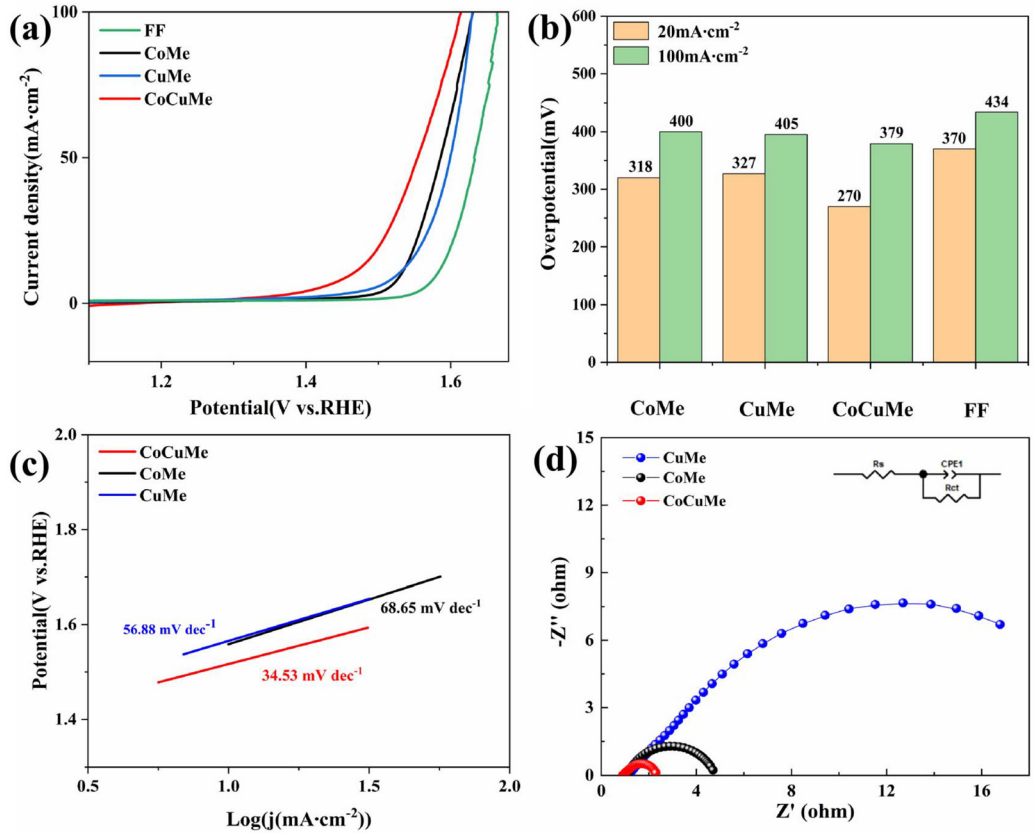

Fig. 4 (a) LSV curves with 100% IR compensation of CoCuMe, CoMe, CuMe, and FF. (b) Overpotentials of CoCuMe, CoMe, CuMe, and FF at current densities of 20 mA cm^{-2} and 100 mA cm^{-2}, respectively. (c) The Tafel curves of CoCuMe, CoMe, and CuMe. (d) Impedance profiles of CoCuMe, CoMe, and CuMe.

Therefore, this study conducted stability testing on CoCuMe using the chronopotentiostatic method (i–t). As shown in Fig. 5a, after 100 hours of chronopotentiostatic testing at a current density of 100 mA cm^{-2}, the potential of CoCuMe remained stable without a significant decrease, indicating that the catalytic activity for the OER did not significantly change within 100 hours (the potential remained stable between 1.68 V and 1.71 V). As shown in Fig. 5b, a comparison of the LSV curves before and after 100 mA cm^{-2} for 100 h reveals that the LSV curves exhibit no significant changes. This result demonstrates that CoCuMe exhibits excellent stability for OER catalysis.

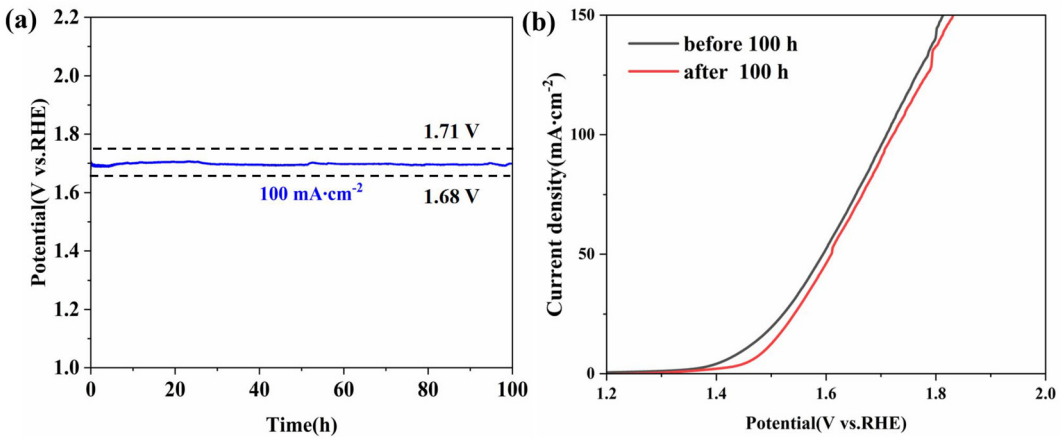

Fig. 5 (a) Time–voltage curve tested for 100 hours at a current density of 100 mA cm^{-2} (without IR compensation). (b) Comparison of LSV curves before and after 100 hours of testing at a current density of 100 mA cm^{-2} without IR compensation.

The electrochemical double layer capacitance (CDL) can be fitted to the electrochemically active surface area.[34] Therefore, CDL tests were performed on the samples. Fig. 6a shows the CV curves of CoCuMe at various scanning rates. The CDL specific size can be calculated from its results. The CV curves of CoMe and CuMe at different rates are shown in Fig. S7. The CDL of CoCuMe is 146.4 mF cm^{-2}, which is higher than those of CoMe (55.1 mF cm^{-2}) and CuMe (19.4 mF cm^{-2}) (Fig. 6b). The fact that CoCuMe has a higher value of CDL implies that there is a higher electrochemically active region, which is due to the unique flower-like structure of the material CoCuMe made of stacked ultrathin nanosheets, which will be beneficial for increasing the quantity of catalytic active sites, thus enhancing the electrocatalytic OER activity.

In order to investigate the reason for exerting the main catalytic activity during the OER process, the XPS characterization of the CoCuMe sample after stability testing (*i–t* method) is hereby carried out. As shown in Fig. 7(a and b), the comparison with CoCuMe before stability testing shows that the increase in the amount of Co^{3+} is particularly prominent, and it can be known that Co^{2+} is further oxidized to generate Co^{3+} during the OER process. The increase in Cu^{2+} content is compared to CoCuMe prior to stability testing. In Fig. 7c, a significant increase in the amount of Fe^{3+} can be seen in the high-resolution Fe 2p XPS spectrum, implying that Fe may also be important activation centers and also indicating the further oxidation of Fe^{2+} during the OER process.[35] Therefore, the addition of Co and Cu to the hydroxymethyl compound materials helps to expose the Fe sites or improve the effectiveness of the Fe sites. As can be seen from Table S4, the four subpeaks located at 529.50 eV, 530.77 eV, 531.7 eV, and 532.8 eV corresponded clearly in the high-resolution O 1s spectra and the adsorption energies were all enhanced by a certain amount with respect to the O 1s spectra prior to the stability test, where the peak appearing at 530.75 eV is the oxygen in the H–O bond. The peak located at 529.5 eV corresponds to the metal oxides formed on the surface of the material, and the peaks appearing at 531.7 eV and 532.8 eV correspond to the oxygen in the indicated adsorbed oxygen and water molecules.[36]Experimental results demonstrate that bimetallic hydroxymethyl compounds were oxidized to (oxygen-containing) hydroxides during the oxygen evolution reaction (OER), forming stable new structures. The electronic structure of the catalyst surface was adjusted by the newly formed non-homogeneous structure, increased the charge densities of cobalt and iron atoms, decreased the Gibbs free energy of the OER intermediates, and improved the OER kinetics, resulting in improved electrocatalytic OER performance.[37,38]

Numerous studies have demonstrated that the reaction between alcohol molecules with surface adsorbed OH* occurs extremely rapidly. Furthermore, in the widely accepted reaction mechanism, OH* serves as the first intermediate in the catalytic cycle of the oxygen evolution reaction. Based on this research, it is recommended to use alcohol molecules to detect the active OH* generated on oxides and (oxy)hydroxides in the oxygen evolution reaction. Our experimental results indicate that, despite significant differences in reaction conditions and catalyst structures, OH* generated in the oxygen evolution reaction can also oxidize alcohol molecules, analogous to that on metal surfaces. Thus, alcohol molecules can be effectively used to detect the electrophilic OH* generated in the catalytic cycle of the oxygen evolution reaction.[39]

As shown in Fig. 8, three different catalysts were tested under the same conditions using LSV measurements in 1 M KOH and 1 M (KOH + MeOH) solutions. The differences between the two curves primarily depend on the coverage of OH* on the catalyst surface. When the production of OH* during the OER process exceeds its consumption, the reaction current in the MOR is significantly higher than the reaction current in a KOH only electrolyte solution. That is, the area between the two LSV curves is larger. By integrating the area corresponding to the two LSV reactions, the values in Fig. 8(a–c) are 3.31, 9.21, and 13.06, respectively. Therefore, OH* is most extensively covered on CoCuMe, indicating that CoCuMe has the most suitable adsorption capacity for OH*, thereby enhancing its OER catalytic performance.[39]

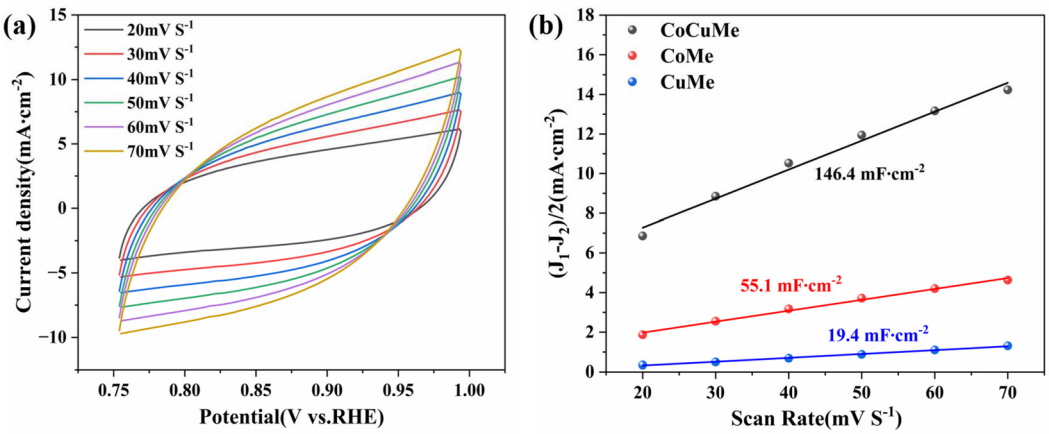

Fig. 6 (a) CV curves of CoCuMe and (b) CDL of CoCuMe, CoMe and CuMe.

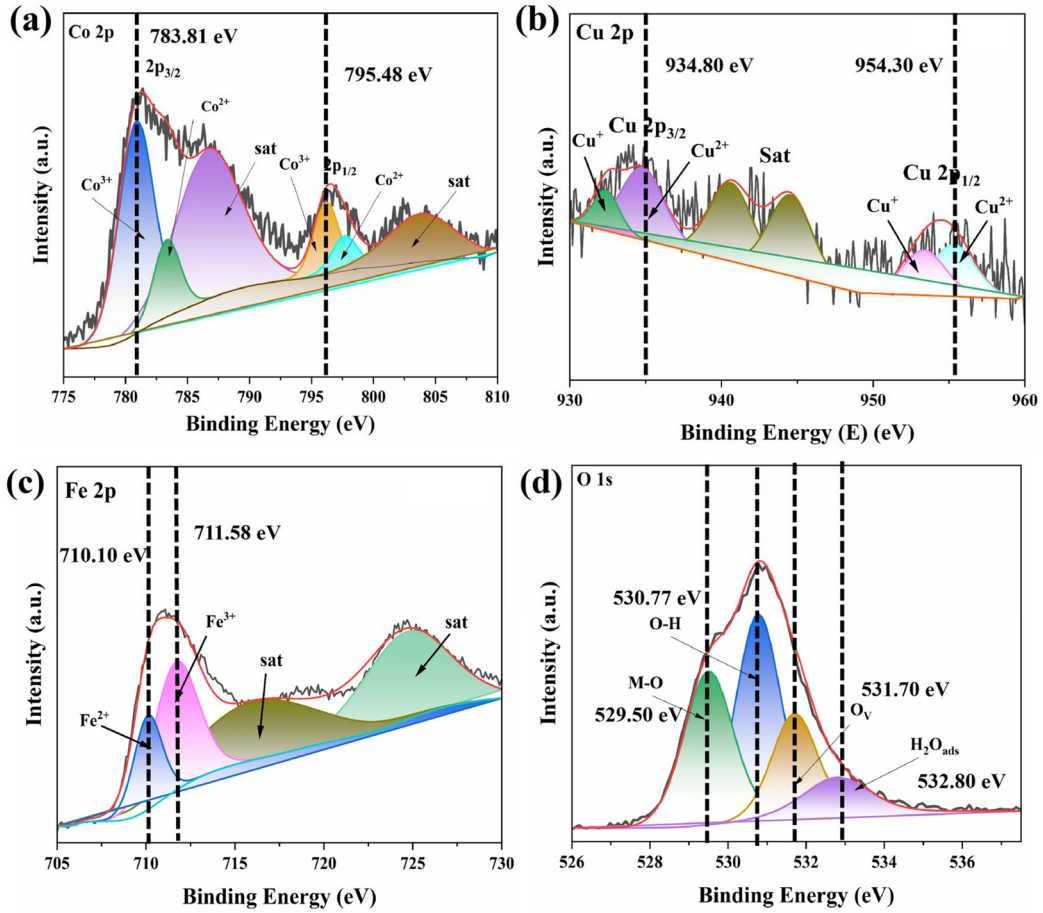

Fig. 7 High-resolution XPS spectra of (a) Co 2p, (b) Cu 2p, (c) Fe 2p, and (d) O 1s for CoCuMe after chronometric testing at a current density of 100 mA cm^{-2} for 100.

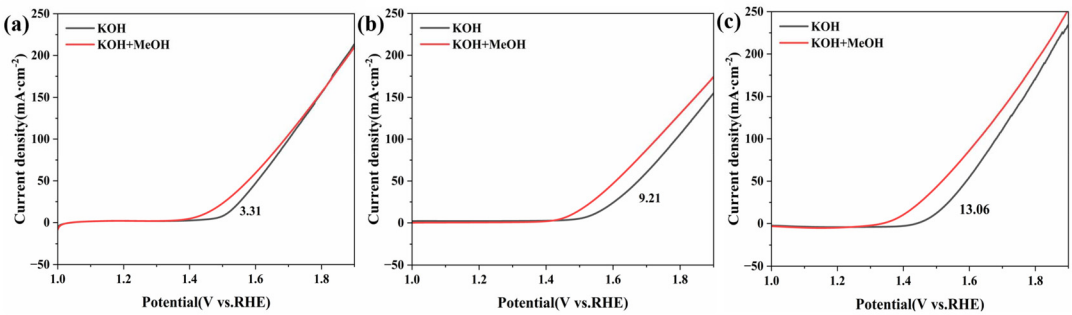

Fig. 8 The LSV curves of (a) CoMe, (b) CuMe, and (c) CoCuMe in 1 M KOH and 1 M (KOH + MeOH).

4. Conclusion

We synthesized a flower-like CoCuMe OER catalyst *via* a one-step hydrothermal process. This rational approach resulted in outstanding OER catalytic activity. In a 1 M KOH alkaline solution, the voltages were only 270 mV and 379 mV at current densities of 20 mA cm^{-2} and 100 mA cm^{-2}, respectively, and stable operation was maintained for 100 hours at 100 mA cm^{-2}. The reason was that the methoxy anionic groups induced complete surface remodeling, and the flower-like structure formed by the stacking of ultrathin nanosheets provided enough catalytic active sites. Meanwhile, on the basis of Co^{2+} and Cu^{2+}, the adsorption capacity of the intermediate OH* and the conductivity are improved, which leads to the final OER catalytic results. This work shows that the combination of multiple variable metal cations and methoxy anions can enhance the performance of OER catalysts, and the one-step hydrothermal method is more efficient than other catalyst

preparation methods. This facilitates the advancement of catalysts in other relevant fields.

Author contributions

Pan Yang: writing – original draft, validation, methodology, and conceptualization. Congmin Fan: writing – review & editing, project administration, and funding acquisition. Tiancheng Feng: data analysis and investigation. Haoyu Peng: visualization and investigation. Xiaolian Xu: visualization and investigation. Guiqi Gao: investigation and supervision.

Conflicts of interest

The authors declare that they have no known competing financial interests or personal relationships that could have appeared to influence the work reported in this paper.

Data availability

Data will be made available on request.

Supplementary information (SI) is available. See DOI: https://doi.org/10.1039/d5dt02687c.

References

1 Z. Zhu, W. Hu, X. Wu, Q. Zhang, Y. Hu, Q. Yan, X. Wang and W. Yuan, *In situ* self-assembled macroporous interconnected nanosheet arrays of Ni-1,3,5-benzenetricarboxylate metal-organic framework on Ti mesh as high-performance oxygen evolution electrodes, *J. Colloid Interface Sci.*, 2023, **639**, 274–283, DOI: 10.1016/j.jcis.2023.02.079.

2 H. Dai, A. H. Zhang, A. C. Wu, T. Y. Wu, X. Xiao and C. J. Zhou, The reverse water gas shift with photo-thermocatalytic synergistic catalysis by CuCe-LDO, *Mater. Today Chem.*, 2025, **45**, DOI: 10.1016/j.mtchem.2025.102648.

3 H. J. W. Li, Y. Lin, J. Y. Duan, Q. L. Wen, Y. W. Liu and T. Y. Zhai, Stability of electrocatalytic OER: from principle to application, *Chem. Soc. Rev.*, 2024, **53**, 10709–10740, DOI: 10.1039/d3cs00010a.

4 J. Z. Jia, Y. T. Wang, Y. Y. Cha, Z. W. Wang, J. F. Huang, D. N. Wang, H. Li, K. L. Guo, J. Li, J. E. Huang, Y. Tang and C. L. Xu, Boosting OER performance of NiFe–MOFs *via* heterostructure engineering: promoted phase transformation and self-optimized dynamic interface electron structure, *Adv. Funct. Mater.*, 2025, **35**, DOI: 10.1002/adfm.202500568.

5 L. X. Feng, A. R. Li, Y. X. Li, J. Liu, L. D. Y. Wang, L. Y. Huang, Y. Wang and X. B. Ge, A highly active CoFe layered double hydroxide for water splitting, *ChemPlusChem*, 2017, **82**, 483–488, DOI: 10.1002/cplu.201700005.

6 O. A. L. Alves, B. S. G. Xavier, W. R. A. S. Lima, L. F. Loguercio, M. Navarro, T. A. S. Soares and G. Machado, Beyond the catalyst: Unveiling the hidden impact of support electrode and deposition method on OER alkaline electrocatalytic data, *Electrochim. Acta*, 2026, **546**, 147794, DOI: 10.1016/j.electacta.2025.147794.

7 X. L. Xu, Y. Dong, Q. W. Hu, N. Si and C. W. Zhang, Electrochemical hydrogen storage materials: state-of-the-art and future perspectives, *Energy Fuels*, 2024, **38**, 7579–7613, DOI: 10.1021/acs.energyfuels.3c05138.

8 S. Sikiru, T. L. Oladosu, T. I. Amosa, J. O. Olutoki, M. N. M. Ansari, K. J. Abioye, Z. U. Rehman and H. Soleimani, Hydrogen-powered horizons: transformative technologies in clean energy generation, distribution, and storage for sustainable innovation, *Int. J. Hydrogen Energy*, 2024, **56**, 1152–1182, DOI: 10.1016/j.ijhydene.2023.12.186.

9 N. T. Suen, S. F. Hung, Q. Quan, N. Zhang, Y. J. Xu and H. M. Chen, Electrocatalysis for the oxygen evolution reaction: recent development and future perspectives, *Chem. Soc. Rev.*, 2017, **46**, 337–365, DOI: 10.1039/c6cs00328a.

10 X. L. Xu, C. M. Fan, P. Yang, T. C. Feng and H. Lv, 3D needle-like heterostructured sulfide FeS/Ni_3S_2/NF toward highly efficient oxygen evolution reaction, *J. Alloys Compd.*, 2025, **1010**, 178136, DOI: 10.1016/j.jallcom.2024.178136.

11 Y. Jiao, Y. Zheng, M. T. Jaroniec and S. Z. Qiao, Design of electrocatalysts for oxygen and hydrogen involving energy conversion reactions, *Chem. Soc. Rev.*, 2015, **44**, 2060–2086, DOI: 10.1039/c4cs00470a.

12 T. T. Liu, Q. Liu, A. M. Asiri, Y. L. Luo and X. P. Sun, An amorphous CoSe film behaves as an active and stable full water-splitting electrocatalyst under strongly alkaline conditions, *Chem. Commun.*, 2015, **51**, 16683–16686, DOI: 10.1039/c5cc06892d.

13 J. Huang, J. Chen, T. Yao, J. He, S. Jiang, Z. Sun, Q. Liu, W. Cheng, F. Hu, Y. Jiang, Z. Pan and S. Wei, CoOOH nanosheets with high mass activity for water oxidation, *Angew. Chem., Int. Ed.*, 2015, **54**, 8722–8727, DOI: 10.1002/anie.201502836.

14 S. Y. Cheng, T. Wang, J. W. Kou, F. Q. Cheng, H. P. Song and H. Z. Zhao, Improving hydrogen production activity of bifunctional CuCoFe-layered double hydroxides for electrocatalytic water splitting: effects of valence state evolution and oxygen vacancies, *Fuel*, 2024, **361**, 130711, DOI: 10.1016/j.fuel.2023.130711.

15 W. Hu, Q. Yan, X. Wang, J. Lu, Q. He, Q. Zhang and W. Yuan, In situ controllably self-assembled CoFe–TDPAT metal-organic framework nanosheet arrays on iron foam as highly efficient bifunctional catalytic electrodes for overall water splitting at large current density, *Adv. Funct. Mater.*, 2025, **35**, 2411904, DOI: 10.1002/adfm.202411904.

16 Y. R. Hao, H. Xue, J. Sun, N. K. Guo, T. S. Song, H. L. Dong, Z. L. Zhao, J. W. Zhang, L. M. Wu and Q. Wang, Achieving superior oxygen evolution of perovskite via phase transition and electrochemical reconstruction strategy, *Energy Environ. Sci.*, 2024, **17**, 12, DOI: 10.1039/d3ee04338j.

17 H. F. Wang, C. Tang, B. Wang, B. Q. Li and Q. Zhang, Bifunctional transition metal hydroxysulfides: room-temperature sulfurization and their applications in Zn-air batteries, *Adv. Mater.*, 2017, **29**, 35, DOI: 10.1002/adma.201702327.

18 B. Zhang, X. Zheng, O. Voznyy, R. Comin, M. Bajdich, M. Garcia-Melchor, L. Han, J. Xu, M. Liu, L. Zheng, F. P. Garcia de Arquer, C. T. Dinh, F. Fan, M. Yuan, E. Yassitepe, N. Chen, T. Regier, P. Liu, Y. Li, P. De Luna, A. Janmohamed, H. L. Xin, H. Yang, A. Vojvodic and E. H. Sargent, Homogeneously dispersed multimetal oxygen-evolving catalysts, *Science*, 2016, **352**, 333–337, DOI: 10.1126/science.aaf1525.

19 M. Luo, Z. Cai, C. Wang, Y. M. Bi, L. Qian, Y. C. Hao, L. Li, Y. Kuang, Y. P. Li, X. D. Lei, Z. Huo, W. Liu, H. L. Wang, X. M. Sun and X. Duan, Phosphorus oxoanion-intercalated layered double hydroxides for high-performance oxygen evolution, *Nano Res.*, 2017, **10**, 5, DOI: 10.1007/s12274-017-1437-2.

20 P. Liu and E. J. M. Hensen, Highly efficient and robust Au/$MgCuCr_2O_4$ catalyst for gasphase oxidation of ethanol to acetaldehyde, *J. Am. Chem. Soc.*, 2013, **135**, 14032–14035, DOI: 10.1021/ja406820f.

21 H. Y. Yang, Z. L. Chen, P. F. Guo, B. Fei and R. B. Wu, B-doping-induced amorphization of LDH for large-current-density hydrogen evolution reaction, *Appl. Catal., B*, 2020, **261**, DOI: 10.1016/j.apcatb.2019.118240.

22 K. Fan, H. Y. Zou, Y. Lu, H. Chen, F. S. Li, J. X. Liu, L. C. Sun, L. P. Tong, M. F. Toney, M. L. Sui and J. G. Yu, Direct observation of structural evolution of metal chalcogenide in electrocatalytic water oxidation, *ACS Nano*, 2018, **12**(12), 12369–12379, DOI: 10.1021/acsnano.8b06312.

23 D. F. Yan, Y. X. Li, J. Huo, R. Chen, L. M. Dai and S. Y. Wang, Defect chemistry of nonprecious-metal electrocatalysts for oxygen reactionshighly cited paper, *Adv. Mater.*, 2017, **29**, 48, DOI: 10.1002/adma.201606459.

24 X. Dong, Y. Ma, X. Fan, S. Zhao, Y. Xu, S. Liu and D. Jin, Nickel modified two-dimensional bimetallic nanosheets, $M(OH)(OCH_3)$ (M = Co, Ni), for improving fire retardancy and smoke suppression of epoxy resin, *Polymer*, 2021, **235**, 124263, DOI: 10.1016/j.polymer.2021.124263.

25 Q. Jiang, R. Lu, J. Gu, L. Zhang, K. Liu, M. Huang, P. Liu, S. Zuo, Y. Wang, Y. Zhao, P. Ma and Z. Fu, A highly efficient high-entropy metal hydroxymethylate electrocatalyst for oxygen evolution reaction, *Chem. Eng. J.*, 2023, **453**, 139510, DOI: 10.1016/j.cej.2022.139510.

26 M. Wang, Y. Xing, Q. Shi, Y. Ge, M. Xiang, Z. Huang, Q. Xuan, Y. Fan and Y. Zhao, High areal capacity FeS@Fe foam anode with hierarchical structure for alkaline solid-state energy storage, *Adv. Energy Mater.*, 2024, **14**, 16, DOI: 10.1002/aenm.202304060.

27 Y. Zhao, Q. Sun, C. Zhang, F. Liu, L. Wang and G. R. Xu, Self-supported electrocatalysts for high-current-density water/seawater electrolysis, *J. Alloys Compd.*, 2023, **968**, 172286, DOI: 10.1016/j.jallcom.2023.172286.

28 J. Y. He, Y. B. Liu, Y. C. Huang, H. Li, Y. Q. Zou, C. L. Dong and S. Y. Wang, Fe^{2+} induced in situ intercalation and cation exsolution of $Co_{80}Fe_{20}(OH)(OCH_3)$ with rich vacancies for boosting oxygen evolution reaction, *Adv. Funct. Mater.*, 2021, **31**, 2009245, DOI: 10.1002/adfm.202009245.

29 Y. C. Pi, Q. I. Shao, P. T. Wang, F. Lv, S. J. Guo, J. Guo and X. Q. Huang, Trimetallic oxyhydroxide coralloids for efficient oxygen evolution electrocatalysis, *Angew. Chem., Int. Ed.*, 2017, **56**(16), 4502–4506, DOI: 10.1002/anie.201701533.

30 C. S. Lim, C. K. Chua, Z. Sofer, K. Klímova, C. Boothroyd and M. Pumera, Layered transition metal oxyhydroxides as tri-functional electrocatalysts, *J. Mater. Chem. A*, 2015, **3**(22), 11920–11929, DOI: 10.1039/c5ta02063h.

31 Y. H. Lyu, J. Y. Zheng, Z. H. Xiao, S. Y. Zhao, S. P. Jiang and S. Y. Wang, Identifying the intrinsic relationship between the restructured oxide layer and oxygen evolution reaction performance on the cobalt pnictide catalyst, *Small*, 2020, **16**, 1906867, DOI: 10.1002/smll.201906867.

32 F. Kazemzadeh and B. Haghighi, Electrocatalytic activity of Cu-Co prussian blue analogue and its calcined derivatives towards OER, *Solid State Sci.*, 2025, **163**, 107887, DOI: 10.1016/j.solidstatesciences.2025.107887.

33 J. Y. Chen, P. Y. Zhuang, Y. C. Ge, H. Chu, L. Y. Yao, Y. D. Cao, Z. Y. Wang, M. O. L. Chee, P. Dong, J. F. Shen, M. X. Ye and P. M. Ajayan, Sublimation-vapor phase pseudomorphic transformation of template-directed MOFs for efficient oxygen evolution reaction, *Adv. Funct. Mater.*, 2019, **29**(37), 1903875, DOI: 10.1002/adfm.201903875.

34 C. C. L. McCrory, S. Jung, I. M. Ferrer, S. M. Chatman, J. C. Peters and T. F. Jaramillo, Benchmarking hydrogen evolving reaction and oxygen evolving reaction electrocatalysts for solar water splitting devices, *J. Am. Chem. Soc.*, 2015, **137**(13), 4347–4357, DOI: 10.1021/ja510442p.

35 G. Solomon, A. Landstrom, R. Mazzaro, M. Jugovac, P. Moras, E. Cattaruzza, V. Morandi, I. Concina and A. Vomiero, $NiMoO_4$@Co_3O_4 core-shell nanorods: in situ catalyst reconstruction toward high efficiency oxygen evolution reaction, *Adv. Energy Mater.*, 2021, **11**, 2101324, DOI: 10.1002/aenm.202101324.

36 Q. Y. Liu, H. Wang, X. N. Wang, R. Tong, X. L. Zhou and X. N. Peng, Bifunctional $Ni_{1-x}Fe_x$ layered double hydroxides/Ni foam electrodes for high-efficient overall water splitting: a study on compositional tuning and valence state evolution, *Int. J. Hydrogen Energy*, 2017, **42**, 5560–5568, DOI: 10.1016/j.ijhydene.2016.06.056.

37 H. Li, S. Yang, W. Wei, M. Zhang, Z. Jiang, Z. Yan and J. Xie, Chrysanthemum-like FeS/Ni_3S_2 heterostructure nanoarray as a robust bifunctional electrocatalyst for overall water splitting, *J. Colloid Interface Sci.*, 2022, **608**, 536–548, DOI: 10.1016/j.jcis.2021.09.121.

38 P. Wang, R. Qin, P. Ji, Z. Pu, J. Zhu, C. Lin, Y. Zhao, H. Tang, W. Li and S. Mu, Synergistic coupling of Ni nanoparticles with Ni_3C nanosheets for highly efficient overall water splitting, *Small*, 2020, **16**, 37, DOI: 10.1002/smll.202001642.

39 H. B. Tao, Y. H. Xu, X. Huang, J. Z. Chen, L. J. Pei, J. M. Zhang, J. G. G. Chen and B. Liu, A general method to probe oxygen evolution intermediates at operating conditions, *Joule*, 2019, **3**(6), 1498–1509, DOI: 10.1016/j.joule.2019.03.012.